

# Predicting the microstructural evolution in a multi-layered corrosion resistant coating on a Ni-base superalloy

Pillai, Rishi; Taylor, Mary; Galiullin, T.; Chyrkin, Anton; Wessel, E.; Evans, Hugh; Quadackers, Willam

DOI:

[10.1080/09603409.2017.1396650](https://doi.org/10.1080/09603409.2017.1396650)

License:

None: All rights reserved

*Document Version*

Peer reviewed version

*Citation for published version (Harvard):*

Pillai, R, Taylor, M, Galiullin, T, Chyrkin, A, Wessel, E, Evans, H & Quadackers, W 2018, 'Predicting the microstructural evolution in a multi-layered corrosion resistant coating on a Ni-base superalloy', *Materials at High Temperatures*, vol. 35, no. 1-3, pp. 78-88. <https://doi.org/10.1080/09603409.2017.1396650>

[Link to publication on Research at Birmingham portal](#)

## **Publisher Rights Statement:**

Eligibility for repository: Checked on 3/5/2017

This is an Accepted Manuscript of an article published by Taylor & Francis in *Materials at High Temperatures* on 10/11/2017, available online: <https://www.tandfonline.com/doi/full/10.1080/09603409.2017.1396650>

## **General rights**

Unless a licence is specified above, all rights (including copyright and moral rights) in this document are retained by the authors and/or the copyright holders. The express permission of the copyright holder must be obtained for any use of this material other than for purposes permitted by law.

- Users may freely distribute the URL that is used to identify this publication.
- Users may download and/or print one copy of the publication from the University of Birmingham research portal for the purpose of private study or non-commercial research.
- User may use extracts from the document in line with the concept of 'fair dealing' under the Copyright, Designs and Patents Act 1988 (?)
- Users may not further distribute the material nor use it for the purposes of commercial gain.

Where a licence is displayed above, please note the terms and conditions of the licence govern your use of this document.

When citing, please reference the published version.

## **Take down policy**

While the University of Birmingham exercises care and attention in making items available there are rare occasions when an item has been uploaded in error or has been deemed to be commercially or otherwise sensitive.

If you believe that this is the case for this document, please contact [UBIRA@lists.bham.ac.uk](mailto:UBIRA@lists.bham.ac.uk) providing details and we will remove access to the work immediately and investigate.

# Predicting the microstructural evolution in a multi-layered corrosion resistant coating on a Ni-base superalloy

R. Pillai<sup>a,\*</sup>, M.P. Taylor<sup>b</sup>, T. Galiullin<sup>a</sup>, A. Chyrkin<sup>a</sup>, E. Wessel<sup>a</sup>, H. Evans<sup>b</sup>,  
W.J. Quadakkers<sup>a</sup>

<sup>a</sup>*Forschungszentrum Juelich GmbH, IEK-2, 52428, Juelich, Germany*

<sup>b</sup>*School of Metallurgy and Materials, University of Birmingham, Birmingham, B15 2TT, UK*

---

---

## Abstract

Protective metallic MCrAlY or diffusion type (NiAl) coatings enhance the oxidation and corrosion resistance of the underlying high temperature materials employed in aeroengines and industrial gas turbines by ensuring the growth of a slowly growing protective alumina scale. However, a chromia forming coating would provide a better resistance against sulphur induced corrosive attack. A hybrid coating system combining both chromia and alumina forming coating layers would provide optimum protection in oxidising-sulphidising environments.

The microstructural stability and applicability of such a coating system (SmartCoat) containing alternate layers rich in chromium and aluminium respectively on the Ni-base superalloy CMSX-4 was evaluated after various exposure times at 800 °C. Scanning electron microscopy (SEM) and electron microprobe analyses (EPMA) provided the element concentrations. Phases were identified by electron backscatter diffraction (EBSD), and correlated with SEM and high-resolution TEM/EDX analyses. A computational approach was employed to describe the mechanisms of the phase transformations occurring in the coating system.

---

\*Corresponding author

*Email address:* r.pillai@fz-juelich.de (R. Pillai)

**Keywords:** Ni-base alloy, pre-oxidation, carbides, carbide-free-zone, diffusion

## 1. Introduction

Coated Ni-base superalloys combine the excellent creep rupture strength of superalloys with the high oxidation and corrosion resistance of overlay coatings or bondcoats. One of the widely used types of coatings are of the MCrAlY (M = Ni, Co) type [1, 2]. These coatings protect the underlying superalloy component (substrate) in industrial gas turbines and jet engines from high temperature oxidation attack. Oxidation protection of these coatings is provided by the formation of a thermally grown oxide (TGO), usually  $\alpha$ -alumina [3], on the coating surface. However, a chromia forming coating would provide better resistance against sulphate induced corrosive attack [4, 5]. A hybrid coating system combining both chromia and alumina forming coating layers would provide optimum protection in oxidising-sulphidising environments.

SmartCoat coating systems [6, 7] containing alternate layers rich in chromium and aluminium were recently developed to provide corrosion resistance over a wide range of turbine operating conditions. The purpose of these coating systems is to protect the underlying superalloy from simultaneous degradation by oxidation and type 1 and type 2 hot corrosion attack. The compositional grading of the coating systems results in a complex layered microstructure. An understanding of the dependence of the chemical stability of the coating system on the operational parameters such as temperature and time will assist in their design and compositional optimisation. The microstructural stability and performance of the coatings governs the application-specific selection and development of materials. Furthermore, the compatibility between the coating with the underlying substrate is critical for the long-term stability of the coating system [8]. Extensive experimental testing at relevant temperatures and exposure times is a way to compare different coating systems and aids in choosing the right coating system for a specific application [9]. This involves extensive development costs and time

which thus limits the number of alloys or chemical compositions that can be tested.

The current work evaluates the use of computational methods to model the microstructural evolution in the coating system and the substrate during high temperature exposure. Such a procedure provides the flexibility to analyse the behaviour of different combinations of base metal and coating and to predict the influence of alloy and coating composition on long term performance. This would lead to a substantial reduction in the reduced experimental effort required for coating qualification. Taylor et al. [10] modelled the interdiffusion processes in the coating system evaluated in the present work using the ODIN code [11]. The authors however did not consider the thermodynamics of the system and the concentration dependence of the diffusion coefficients. In the present work, a coupled thermodynamic-kinetic model will be employed to describe the simultaneously occurring oxidation and interdiffusion processes in the multilayered coating on the nickel base substrate CMSX-4. The methodology uses available thermodynamic and kinetic data for all occurring phases from ThermoCalc [12].

## 2. Experimental Procedure

Flat specimens ( $\phi 20$  mm with 5 mm thickness) of the Ni-base superalloy CMSX-4 were first coated with AMDRY 962 (NiCrAlY powder) using high velocity oxygen-fuel (HVOF). This first layer was about 160-200  $\mu\text{m}$  thick. The coating step was followed by annealing under vacuum for 4 h at 1080  $^{\circ}\text{C}$ . The coated surface was grit blasted before vapour aluminising to form an Al-enriched layer (nickel aluminide). The outer aluminised region was removed by grit blasting to prepare the surface for the application of an 80-110  $\mu\text{m}$  thick 50:50 Ni-Cr layer by HVOF. A final grit blasting was performed before the application of a 220-250  $\mu\text{m}$  thick yttria stabilised zirconia layer using air-plasma spraying (APS). The nominal compositions of the coating powders and the substrate CMSX-4 are given in Table 1. Fig 1 shows the BSE-image of

the cross section for the as-received coating system. The individual layers of the coating system are designated in the image.

Discontinuous exposures were carried out in laboratory air at 800 °C for times up to 3000 h. Specimens were removed from the furnace after 10 h, 100 h, 500 h, 1000 h, 2000 h and 3000 h for cross-sectional examination. Before preparing the metallographic cross-sections, the oxidized samples were vacuum impregnated with low viscosity resin to maintain the integrity of the coating layers during sectioning. The plane of the cross-section was aligned perpendicular to the flat surface of the specimen. The mounted samples were ground to 1200 grit with SiC grinding papers and subsequently polished with diamond pastes to 1 μm surface finish. The final polishing step was made using colloidal SiO<sub>2</sub> slurry.

### 3. Characterisation methods

Backscattered electron (BSE) and secondary electron (SE) images were taken from the analyzed areas. The scanning electron microscopy studies (SEM) were carried out using a Zeiss SUPRA 50 VP equipped with an Energy dispersive X-ray (EDX) analysis system by Oxford Instruments for measuring concentration profiles. Electron backscattered diffraction (EBSD) analysis was performed to identify the phases present in each of the coating layers in the as-received state. The orientation maps were acquired using a Zeiss Merlin SEM equipped with a Nordlys EBSD camera and Aztec software package (Oxford instruments).

TEM analysis was performed to corroborate some of the phases identified with EBSD. For the preparation of the TEM specimen a Zeiss Auriga cross beam focused ion beam (FIB) with Ga-ion source was used. The TEM lamella had a thickness of approximately 100 nm and a size of 10 x 10 μm<sup>2</sup>. A high angle annular dark field (HAADF) detector was applied to take images in scanning mode (STEM). For analyzing the chemical composition, energy dispersive X-ray spectroscopy was used (X-Max 80, Inca Energy, Oxford instruments). The microscope was a Zeiss Libra 200 transmission electron microscope (TEM) with

an accelerating voltage of 200 kV.

#### 4. Modelling Procedure

The coupled thermodynamic-kinetic approach to model the simultaneously occurring oxidation, diffusion and dissolution processes in the coating system on CMSX-4 was based on the homogenisation model presented by Larsson et al. [25]. The homogenisation model was implemented in a FORTRAN program using the thermodynamic calculation interface of ThermoCalc [12]. The modelling procedure was modified further to allow the calculations to be run on parallel computing cores [13]. The in-house developed modelling procedure has been described in detail elsewhere [14].

In the present work, the phases  $\gamma$ -FCC,  $\gamma'$ -FCC,  $\beta$  and  $\alpha$ -Cr were considered for the calculations and diffusion was considered to occur in all the considered phases. The model was previously successfully applied by the authors to describe the oxidation induced microstructural evolution in the nickel base alloy 602 CA [15, 16] and in three MCrAlY coating systems [14]. Thermodynamic and kinetic data were taken from the databases TCNi5 [17] and MobNi3 [18], respectively.

The experimentally measured oxidation kinetics [10] were used to define the Cr flux as a boundary condition at the oxide-metal interface. The assumption of symmetry at the centre of the sample provided the second spatial boundary condition of zero flux for all elements. The nominal compositions of the individual coating layers and the base alloy in the as-received state was used as the initial composition at time  $t=0$ . The average concentrations in the aluminide layers were estimated from the EDS measurements and the measured phase fractions (image analysis) of the present phases. The model provided average element concentrations and phase fractions as a function of time and distance.


## 5. Results and Discussion


### 5.1. Characterisation of the as-coated state


The as-received state was thoroughly characterised using EDX, EBSD and TEM analyses. The main aim of these investigations was to identify the phases present in each of the individual layers. Fig. 2(a) shows a forescatter image (generated by electrons reflected off the polished surface) of the interface between the Ni-Cr and the aluminide layers which accentuates the topology of the precipitates. An EBSD mapping of the same region is shown in Fig. 2(b). The phases  $\gamma$  and  $\gamma'$  cannot be distinguished with EBSD due to their similar crystal structure and compositions. In the present work, the two phases were differentiated with the help of additional EDS measurements. The Ni-Cr layer mainly consists of the  $\gamma$ -FCC (Ni) and  $\alpha$ -Cr phases. The interface is interestingly pure FCC (was identified as  $\gamma'$ ) mainly resulting from the interdiffusion processes during the heat treatment steps.

A peculiar finding of the EBSD investigations was the identification of Cr-rich carbides at the interface between the Ni-Cr and aluminide layer. To the best of the knowledge of the present authors, none of the steps in the coating processes are believed to be the sources of carbon. Additionally, since the single crystal superalloy CMSX-4 contains a very small or close to a negligible amount of carbon, it was deemed necessary to confirm the EBSD observations with the help of a TEM-analysis.


Three positions were chosen to cut the TEM lamellae for further analysis (Fig. 3(a)). The lamellae were cut perpendicular to the coating at the substrate-NiCrAlY interface, in the aluminide layer and at the interface between the Ni-Cr and aluminide layer. These lamellae were examined with STEM and the EDX mappings of Cr and C at the respective positions are shown in Fig. 3(b). The substrate-NiCrAlY interface did not show any presence of carbon. The element mapping at position 2 (at the interface between the Ni-Cr and aluminide layer) does indicate the presence of a very small amount of C. However, the mapping at position 3 corroborates



the evidence provided by the EBSD analyses  the presence of Cr-rich carbides in the aluminide layer.

A detailed investigation of the source of carbon responsible for precipitation of these carbides is out of the scope of this paper. Since the coating parameters of the manufacturers are proprietary, the possibility of carbon contamination during the various coating steps cannot be completely eliminated. Furthermore, a chemical analyses of the uncoated CMSX4-specimens was not performed to estimate their carbon content (if any). However, assuming that carbon was present in the substrate specimens, the presence of the carbides in the aluminide layer indicate towards a mechanism suggested by Pillai et al. [19] to explain the presence of carbides in the interdiffusion zone (IDZ) of a nickel aluminide coating on the Ni-base superalloy SC2000. It was shown that the trace amounts of carbon (about 0.014 wt.%) in the superalloy accounted for the carbides in the IDZ. This was attributed to the reduced chemical activity of C at the coating surface induced by increasing Al activity and its resulting diffusion from the substrate towards the coating surface under its activity gradient. The vapour aluminising step in the coating procedure of the present work would induce a similar driving force for carbon transport from the substrate to the coating. It was shown by Pillai et al. [19] with the help of thermodynamic calculations, that the solubility of C is lower in  $\beta$ -NiAl than in  $\gamma$  and  $\gamma'$  phases. It is quite possible that the carbides precipitated at the surface of the NiCrAlY layer in the  $\beta$ -NiAl  during aluminising were then subsequently transported to the outer part of the aluminide layer due to the growth of the aluminide layer. The precise reason and mechanism for the formation of carbides in the aluminide layer cannot however be ascertained in the present work.

The phases  $\gamma$ -FCC and  $\alpha$ -Cr were identified in the NiCrAlY coating. Fig. 4(a) shows a SE-image of the region at the NiCrAlY-substrate interface. An SD mapping of the same region is shown in Fig. 4(b). It was determined by EDS analysis that the FCC phase is  $\gamma'$ . Achar et al.[20] evaluated the temperature dependence of the microstructures of four Co-free NiCrAlY coatings with a Cr concentration of 20wt.% and varying Al concentrations (3-12



wt.%). The phases  $\gamma'$ ,  $\beta$  and  $\alpha - Cr$  were shown to be present in  coating at 950 °C. The microstructure transformed to a  $\gamma$ ,  $\beta$  and  $\alpha$ -Cr above 1000 °C. This is in agreement with the experimental investigations conducted by Taylor et al. [21] who determined the transformation temperature of  $\gamma'+\alpha$  to  $\gamma+\beta$  in the Ni-Cr-Al ternary system to be close to 1000 °C. Fig. 5 shows the Ni-Cr-Al ternary phase diagram at 800 °C calculated with ThermoCalc (TCNI5 database). The nominal composition of the NiCrAlY coating (barring Y) discussed in the current work is plotted in the diagram and is located in the two phase  $\gamma'+\alpha$  region, which confirms the experimental observations.

The calculated phase distribution for the as-received state is shown in  8. The model correctly predicted the phases in each of the coating layers at 800°C except at the interface between the Ni-Cr and aluminide layers. The formation of a  $\gamma'$  layer at this interface is probably a result of the various heat treatment steps (at higher temperatures than 800 °C) performed during the coating process. These heat treatment steps were not exactly known  and therefore not considered in the model.

## 5.2. Microstructural evolution during exposure

The exposure at 800 °C induced various microstructural changes in the coating system. The temporal evolution of these changes and their mechanisms will be discussed with the help of modelling results. To understand the phase transformations occurring in the coating layers caused by interdiffusion processes during exposures, the driving forces for diffusion were evaluated in terms of the activity gradients of the elements (primarily Ni, Cr and Al). The temporal evolution of the activity profiles of Ni, Cr and Al is shown in Figs. 9(a), 9(b), 9(c) respectively.

The activity profile of Ni in the as-received state clearly indicates a trough in the aluminide layer, which results in Ni diffusing from the Ni-Cr layer and the NiCrAlY layer to the aluminide layer. With increasing exposure times, the activity of Ni gradually increases in the aluminide layer. The drop in Ni activity in the NiCrAlY layers is however compensated by the diffusion of Ni from the

substrate towards the NiCrAlY, which is usually observed during interdiffusion in NiCrAlY bond coats on Ni-base superalloys [22]. The activity profiles of Al in the as-received state suggest that Al will diffuse from the aluminide layer to the Ni-Cr layer on the left and to the NiCrAlY layer on the right. On the other hand, Cr will diffuse in the opposite direction from the Ni-Cr to the aluminide layer. The diffusion of Cr and Al from the NiCrAlY layer towards the substrate is a commonly observed phenomenon occurring during interdiffusion between NiCrAlY bond coats and the underlying Ni-base superalloy substrates during high temperature exposure [23]. The activity of Cr in the aluminide layer increases with time due to continuing transport of Cr from the Ni-Cr and the NiCrAlY layers but reduces below its value before exposure between 1000 h and 3000 h. The increase in Cr activity up to about 1000 h in the aluminide layer results in a decreased driving force for its diffusion. The reduction in Cr activity in the aluminide layer after 1000 h means that it continues to diffuse to the aluminide layer. The decrease in Cr activity correlates to the complete dissolution of the  $\beta$ -phase in the aluminide layer (after about 1700 h)

The calculated phase distribution in the multilayered coating on the CMSX-4 substrate after 3000 h of discontinuous exposure at 800 °C is shown in Fig. 10. The microstructure at the NiCrAlY-substrate interface was observed to be not influenced by 3000 h of exposure at 800°C (except for minimal interdiffusion), which is expected due to the low temperature and the relatively low activity gradients. This interface will hence not be discussed further. The microstructural evolution in the Ni-Cr and aluminide layers and at the interface between the Ni-Cr and aluminide layers and at the interface between the aluminide and NiCrAlY layers will be discussed in the following sections.

### 5.2.1. Interface between the Ni-Cr and aluminide layers

The SE-images of the region at the interface between the Ni-Cr and aluminide layers after 500 h, 2000 h and 3000 h of discontinuous exposure at 800 °C are shown in Fig. 6. There is clear evidence of the enrichment of  $\alpha$ -Cr (darker phase in the Ni-Cr layer) at the interface between the Ni-Cr

and aluminide layers. The formation of  $\gamma'$  at this interface was observed in the as-received state (Fig. 2) and this layer is retained even after 3000 h, as confirmed by EDS analyses. The model has predicted the formation of  $\alpha$ -Cr in the Ni-Cr layer and the enrichment of  $\gamma'$  at the interface between the Ni-Cr and aluminide layers (Fig. 10). The temporal evolution of the molar fraction of the  $\alpha$ -Cr phase at the interface between the Ni-Cr and aluminide layers is shown in Fig. 11. The phase fraction of  $\alpha$ -Cr increases faster up to about 500 h and then slows down due to the expected decrease in the driving force for diffusion with diminishing activity gradients.

The formation of a Si-rich phase at the interface was observed in the specimens after 2000 h and 3000 h of exposure at 800°C. This phase was identified with EBSD analyses as  $\text{Cr}_3\text{Ni}_2\text{Si}$ . The calculated Si-activity profiles at different times show that Si diffuses from the Ni-Cr layer to the aluminide layer and enriches at the interface (Fig. 12). The mechanism of the precipitation of this phase is similar to the formation of  $\alpha$ -Cr at that interface. There is no thermodynamic description for this phase in the currently available databases from ThermoCalc. Hence, it could not be considered in the calculation.

### 5.2.2. Aluminide coating layer

The aluminide coating layer consisted of the  $\beta$  and the  $\alpha$ -Cr phases in the as-received state (Fig. 2(a)). The experimentally determined (EBSD) phase distribution in the aluminide layer after 3000 h at 800°C shown in Fig. 7(b) indicates that the  $\beta$ -phase is completely dissolved. The coating consists of the  $\gamma'$  and  $\alpha$ -Cr phases which was additionally confirmed by EDS analyses. The continuing diffusion of Al towards the Ni-Cr and the NiCrAlY layers and the counter diffusion of Ni from the Ni-Cr layer, as can be inferred from the activity profiles shown in Figs. 9(b), 9(a), results in the dissolution of the  $\beta$ -phase. The temporal evolution of the maximum molar fraction of the  $\beta$ -NiAl phase is shown in Fig. 11. The  $\beta$ -phase is completely dissolved in the aluminide layer after about 1700 h. This is in agreement with experimental results where the presence of

$\beta$ -phase was confirmed in the specimen discontinuously exposed for 1000 h (not shown here) and was found to be dissolved in the specimen after 2000 h of discontinuous exposure at 800 °C.

### 5.2.3. Diffusion path

To better visualise the occurring interdiffusion processes in the coating system, a diffusion path in terms of the calculated compositions of Ni, Cr and Al in the Ni-Cr, aluminide and NiCrAlY layers after 3000 h of discontinuous exposure at 800 °C was plotted on the calculated ternary Ni-Cr-Al phase diagram after exposure at 800 °C. Although Si might play a role on the thermodynamic equilibria of the system, it was assumed that the diffusion path would not be strongly affected by it (except at the interface between the Ni-Cr and aluminide layers due to the formation of the  $\text{Cr}_3\text{Ni}_2\text{Si}$  phase). A BSE-image of the multilayered coating system after 3000 h of discontinuous exposure at 800 °C is shown in Fig. 13(a). The numbers represent the interdiffusion zones in the multilayered coating formed during exposure. The diffusion path is shown in Fig. 13(b) and the corresponding positions shown in the BSE-image of Fig. 13(a) are marked along the path.

The depletion of Cr at the interface between the TBC and the Ni-Cr layer as a result of its oxidation at the surface results in dissolution of the  $\alpha$ -Cr phase and this zone is located in the single phase  $\gamma$  region (position 1). Moving towards the right with increasing Cr concentration, the two phase  $\beta$ - $\alpha$ -Cr region is reached in the Ni-Cr layer (position 2). The continuous loss of Ni from the Ni-Cr layer to the aluminide layer results in a three phase region ( $\gamma+\gamma'+\alpha$ -Cr) at the interface between the Ni-Cr and aluminide layers (position 3). Position 4 is located in the single phase  $\gamma'$ -region due to the enrichment of  $\gamma'$  in the aluminide layer to the right of the interface between the Ni-Cr and aluminide layers, as was observed experimentally 7(b). Position 5 traverses back to the two phase  $\gamma'+\alpha$ -Cr region corresponding to the as-received composition of the NiCrAlY layer. Although some assumptions were made (exclusion of Si and its influence on the phase equilibria), the diffusion path allowed the visualisation

of the various phase transformations occurring in the multilayered coating on CMSX-4 during high temperature exposure induced by oxidation and diffusion processes in a single diagram.

## 6. Summary and conclusions

The microstructural stability of a multilayered coating system (Ni-Cr, aluminide and NiCrAlY layers) on the nickel base superalloy CMSX-4 during exposure at 800°C was investigated. The as-received state of the coating layers was evaluated and the phases present in each of the layers were identified by EDS, EBSD and TEM analyses. The Ni-Cr layer consisted of the  $\gamma$  and  $\alpha$ -Cr phases and the aluminide layer was mainly  $\beta$ -NiAl with some  $\alpha$ -Cr precipitates. A  $\gamma'$ + $\alpha$ -Cr microstructure was identified in the NiCrAlY layer, which is commonly observed in Co-free overlay bond coats at low temperatures ( $T < 1000^\circ\text{C}$ ).

The driving forces for the diffusion of mainly Ni, Cr and Al between the coating layers was explained with their calculated activity profiles. Ni and Cr diffused from the Ni-Cr and the NiCrAlY layers towards the aluminide layer. Al diffused from the aluminide layer to the Ni-Cr and NiCrAlY layers. These diffusion processes resulted in precipitation of  $\alpha$ -Cr at the interface between the Ni-Cr and aluminide layers and dissolution of  $\beta$ -NiAl in the aluminide layer. The experimentally observed formation of the Si-rich phase  $\text{Cr}_3\text{Ni}_2\text{Si}$  could not be described by the model due to its missing thermodynamic description in the currently available thermodynamic databases (ThermoCalc).

- [1] H. Nickel, D. Clemens, W. Quadackers, L. Singheiser, 'Development of NiCrAlY Alloys for Corrosion-Resistant Coatings and Thermal Barrier Coatings of Gas Turbine Components', Transactions of the ASME 121 (1999) 384–387.
- [2] W. Quadackers, V. Shemet, D. Sebold, R. Anton, E. Wessel, L. Singheiser, 'Oxidation characteristics of a platinumized MCrAlY bond coat for TBC systems during cyclic oxidation at 1000 °C', Surface and Coatings Technology 199 (2005) 77–82.
- [3] D. Naumenko, V. Shemet, L. Singheiser, W. Quadackers, 'Failure mechanisms of thermal barrier coatings on MCrAlY-type bondcoats associated with the formation of the thermally grown oxide', Journal of Material Science 44 (2009) 1687–1703.
- [4] J. Goebel, F. Pettit, G. Goward, 'MECHANISMS FOR HOT CORROSION OF NICKEL-BASE ALLOYS', Metallurgical Transactions 4 (1973) 261–278.
- [5] F. Pettit, G. Meier, 'Oxidation and Hot Corrosion of Superalloys', Superalloys, The Metallurgical Society (1984) 651–687.
- [6] J. Nicholls, N. Simms, W. Chan, H. Evans, 'Smart overlay coatings – concept and practice', Surface and Coatings Technology 149 (2002) 236–244.
- [7] M. Taylor, H. Evans, S. Gray, J. Nicholls, 'Modelling of the interdiffusion and oxidation of a multilayered chromia forming thermal barrier coating', Materials and Corrosion 68 (2011) 215–219.
- [8] B. Pint, I. Wright, W. Lee, Y. Zhang, D. Prüssner, K. Alexander, 'Substrate and bond coat compositions: factors affecting alumina scale adhesion', Materials Science and Engineering A 245 (1998) 201–211.

- [9] B. Pint, S. Dryepondt, A. Rouaix-Vande Put, Y. Zhang, ‘Mechanistic-Based Lifetime Predictions for High-Temperature Alloys and Coatings’, *JOM, TMS* 64 (1998) 1454–1460.
- [10] M. Taylor, P. Smith, H. Evans, ‘Modelling of the interdiffusion and oxidation of a multilayered chromia forming thermal barrier coating’, *Materials and Corrosion* 68 (2016) 215–219.
- [11] W. Pragnell, H. Evans, ‘A finite-difference model to predict 2D depletion profiles arising from high temperature oxidation of alloys’, *Modelling Simul. Mater. Sci. Eng.* 14 (2006) 733–740.
- [12] B. Jansson, M. Schalin, M. Selleby, B. Sundman, ‘The Thermo-Calc Database System’, in: C. Bale, et al. (Eds.), *ComputeFr Software in Chemical and Extractive Metallurgy*, Canadian Inst Mining, Metallurgy and Petroleum, 1993, pp. 57–71.
- [13] R. Pillai, T. Galiullin, A. Chyrkin, W. Quadackers, ‘Methods to increase computational efficiency of CALPHAD-based thermodynamic and kinetic models employed in describing material degradation’, *CALPHAD* 53 (2016) 62–71.
- [14] R. Pillai, W. Sloof, A. Chyrkin, L. Singheiser, W. Quadackers, ‘A new computational approach for modelling the microstructural evolution and residual lifetime assessment of MCrAlY coatings’, *Materials at High Temperatures* 32 (2015) 57–67.
- [15] A. Chyrkin, R. Pillai, H. Ackermann, H. Hattendorf, S. Richter, W. Nowak, D. Grüner, W. Quadackers, ‘Modeling carbide dissolution in alloy 602 CA during high temperature oxidation’, *Corrosion Science* 96 (2015) 32–41.
- [16] A. Chyrkin, W. Sloof, R. Pillai, T. Galiullin, D. Grüner, W. Quadackers, ‘Modelling compositional changes in nickel base-alloy 602 CA during high temperature oxidation’, *Materials at High Temperatures* 32 (2015) 102–112.

- [17] Thermo-Calc, 'TCNI5, TCS Ni-based superalloys Database' (2011).
- [18] Thermo-Calc, 'MOBNI3, TCS Ni-alloys Mobility Database' (2015).
- [19] R. Pillai, A. Chyrkin, D. Grüner, W. Nowak, N. Zheng, A. Kliewe, W. Quadakkers, 'Carbides in an aluminised single crystal superalloy: Tracing the source of carbon ', *Surface and Coatings Technology* 288 (2016) 15–24.
- [20] D. Achar, R. Munoz-Arroyo, L. Singheiser, W. Quadakkers, 'Modelling of phase equilibria in MCrAlY coating systems', *Surface and Coatings Technology* 187 (2004) 272–283.
- [21] M. Fleetwood, Influence of nickel-base alloy composition on the behaviour of protective aluminide coatings, *Journal of the Institute of Metals* 81 (1970) 451–470.
- [22] J. Nesbitt, R. Heckel, 'Modelling Degradation and Failure of Ni-Cr-Al Overlay Coatings', *Metallurgical and Protective Coatings* 119 (1987) 281–290.
- [23] E. Lee, D. Chartier, R. Biederman, R. Sisson Jr., 'Modelling the Microstructural Evolution and Degradation of M-Cr-Al-Y Coatings during high temperature oxidation', *Surface and Coatings Technology* 32 (1987) 19–39.



Table 1: Nominal composition of the coating layers and the substrate (CMSX-4) in wt %

Element	Cr	Co	Al	Ta	W	Ti	Mo	Re	Si	Y	Hf	Ni
Ni-Cr layer	49	-	-	-	-	-	-	-	2.0	-	-	49
AMDRY 962	22.0	-	10.0	-	-	-	-	-	-	1.0	-	Bal.
Substrate (CMSX-4)	6.5	9.6	5.6	6.5	6.4	1.0	0.6	3.0	-	-	0.1	Bal.

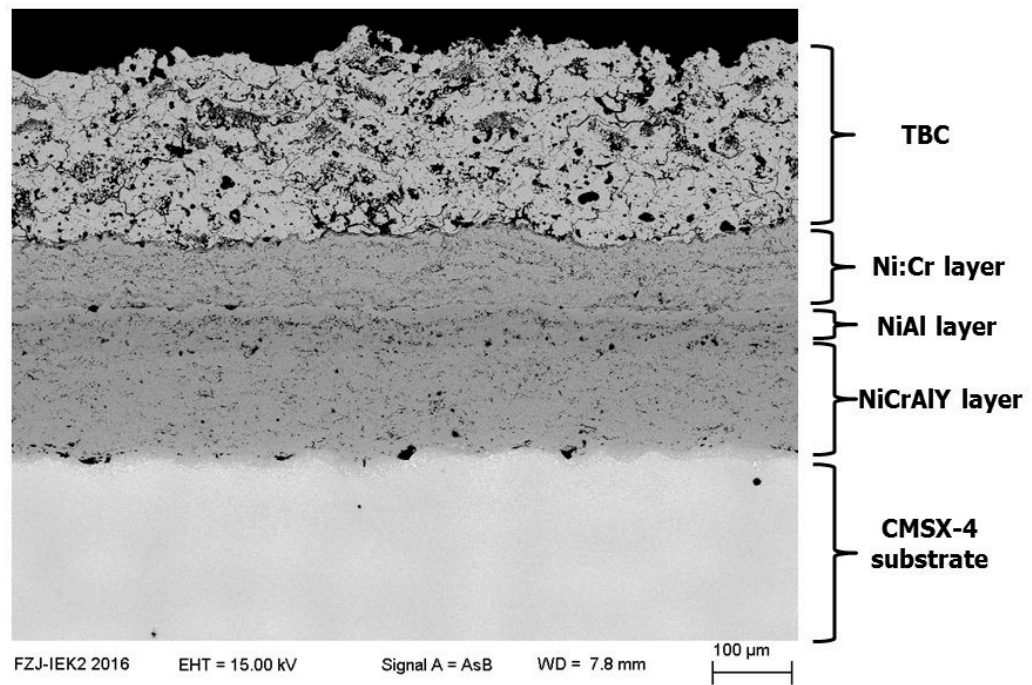


Figure 1: BSE image of the cross section of the as-received material of the coating system

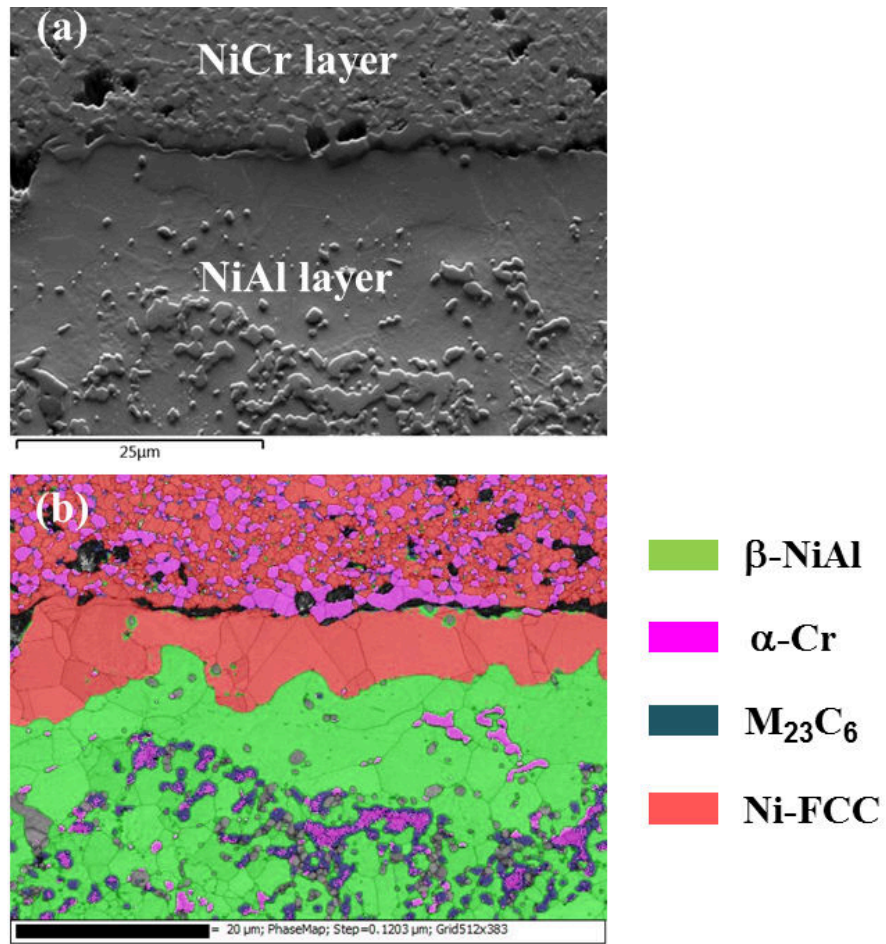
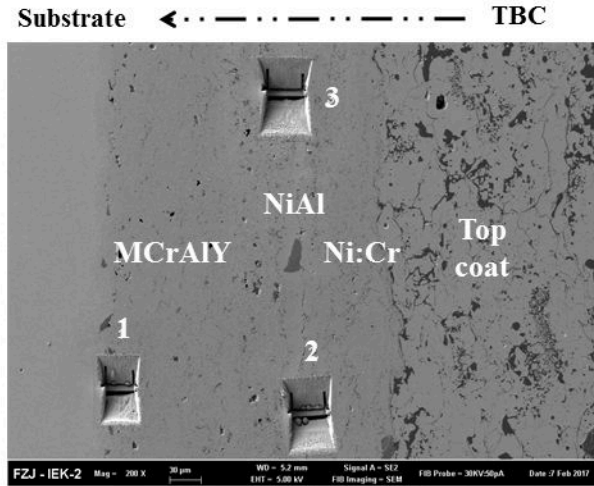
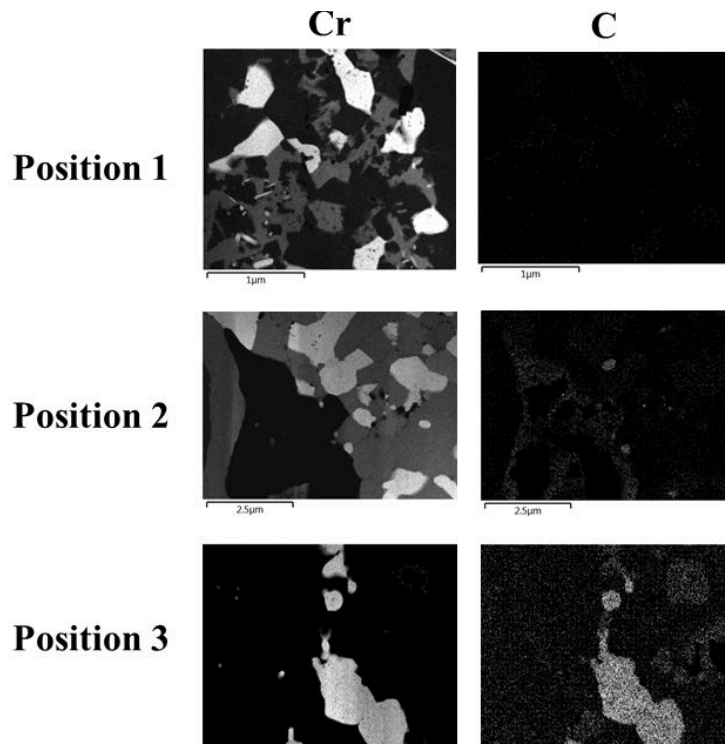


Figure 2: (a) Forescatter image (generated from the electrons reflected off the specimen) of the region at the interface between the Ni-Cr and aluminide layers showing the topology of the phases. (b) The phases identified by EBSD in the same region of Fig. 2(a) in the material of the as-received coating on CMSX-4. The FCC phase was identified as  $\gamma'$  with EDS analyses.



(a)



(b)

Figure 3: (a) SE-image showing the positions of the TEM lamellae and (b) EDX maps of Cr and C in the TEM lamellae at the respective positions in the material of the as-received multilayered coating on CMSX-4.

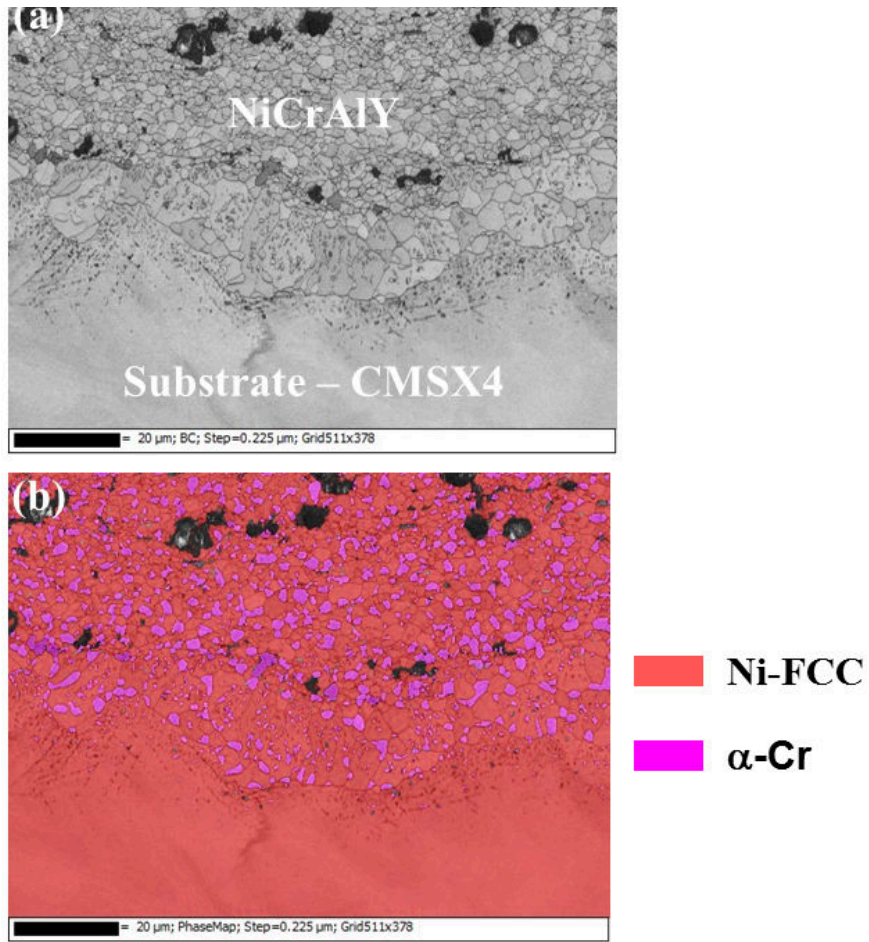


Figure 4: (a) SE-image of the region at the interface between NiCrAlY coating and CMSX-4 substrate. (b) The phases identified by EBSD in the same region of Fig.(a) at the interface between NiCrAlY coating and CMSX-4 substrate. The FCC phases in the substrate were identified as  $\gamma/\gamma'$  with EDS analyses.

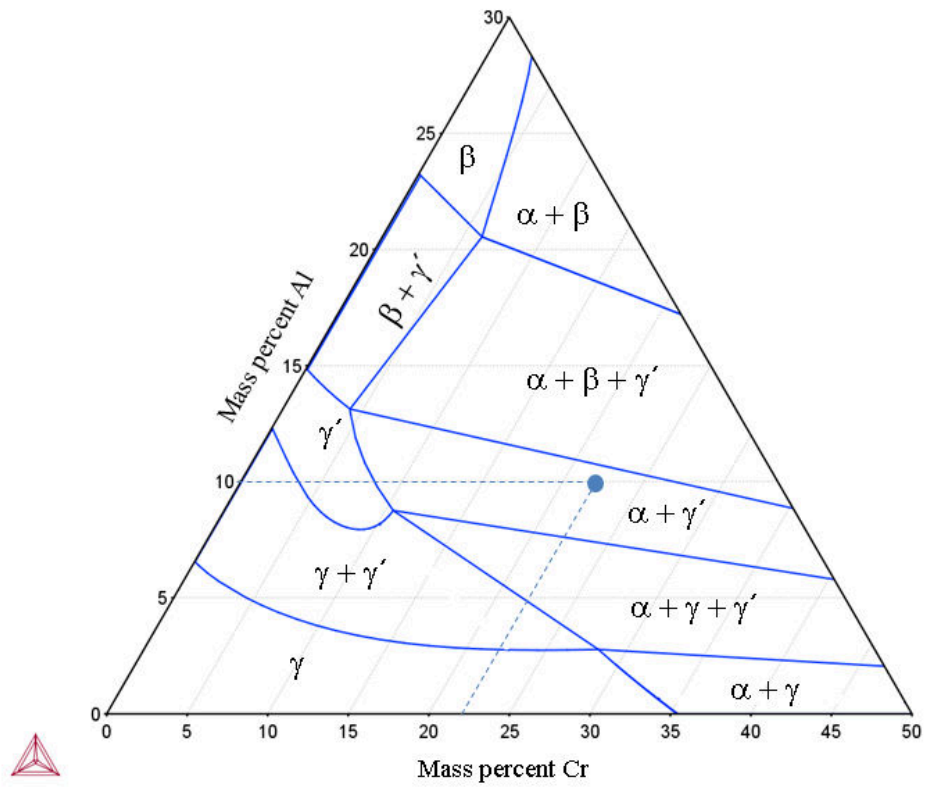


Figure 5: NiCrAl ternary phase diagram at 800 °C calculated with ThermoCalc (TCNI5 database). The inserted symbol designates the nominal composition of the NiCrAlY coating AMDRY 962.

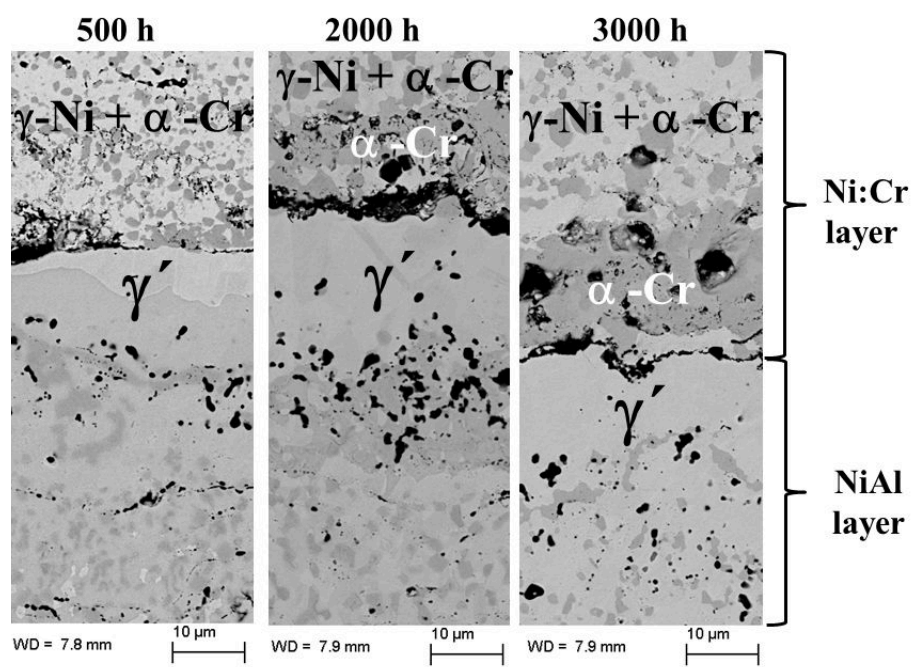


Figure 6: Temporal evolution of the phase distribution at the interface between the Ni-Cr and aluminide layers during discontinuous exposure at 800 °C in laboratory air.

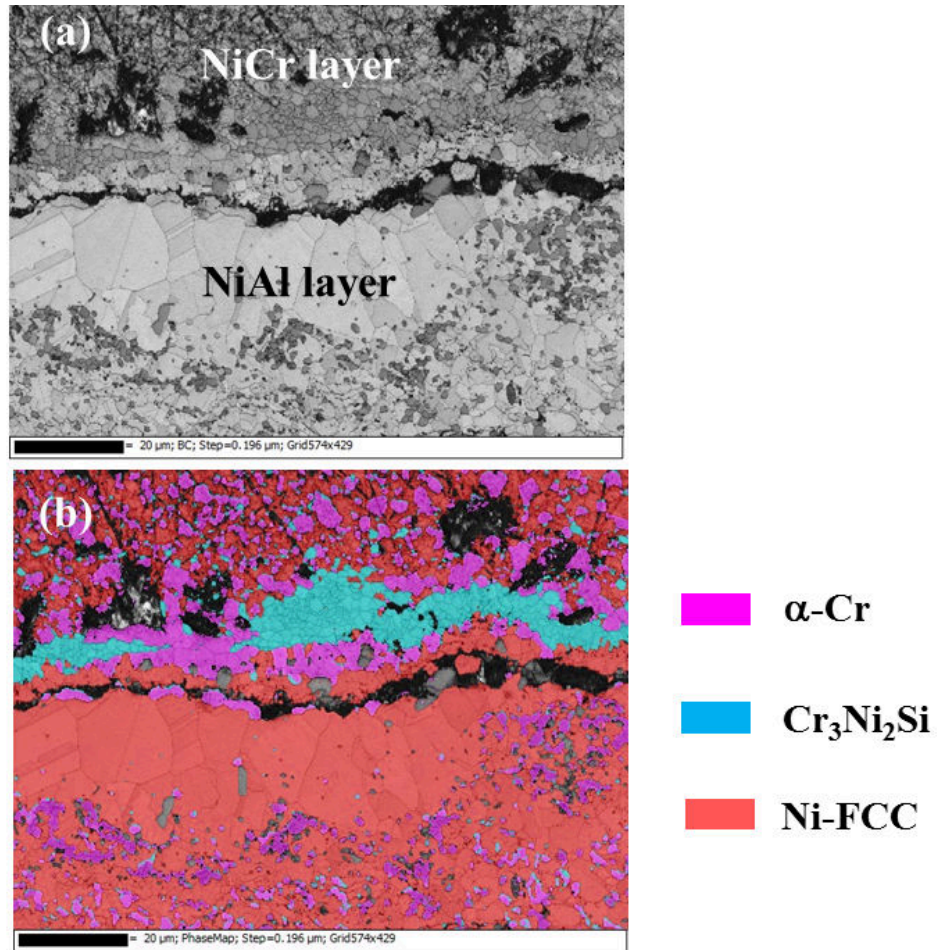


Figure 7: (a) SE-image of the region at the interface between the Ni-Cr and aluminide layers. (b) The phases identified by EBSD in the same region of Fig. 7(a) after discontinuous exposure in laboratory air at 800 °C. The FCC phase was identified as  $\gamma'$  with EDS analyses.

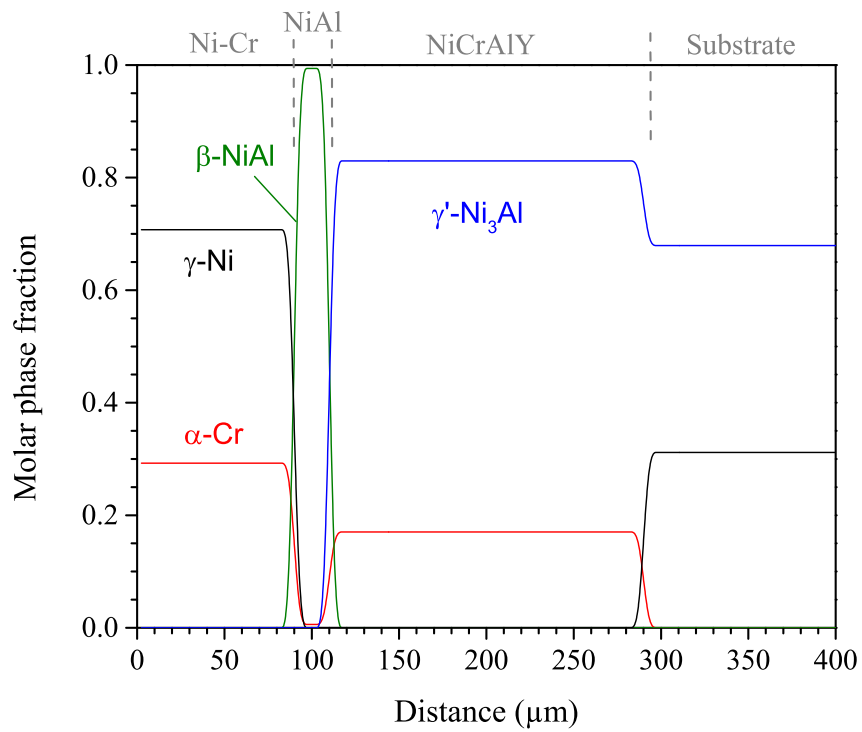
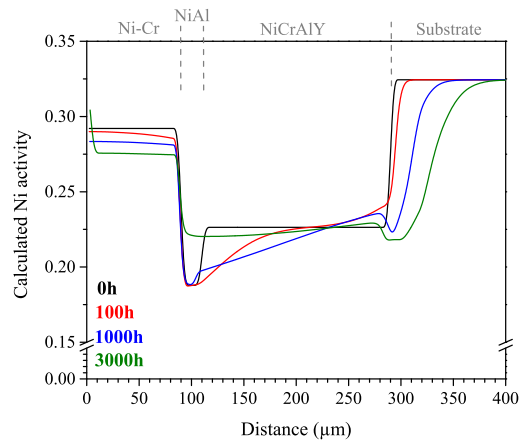
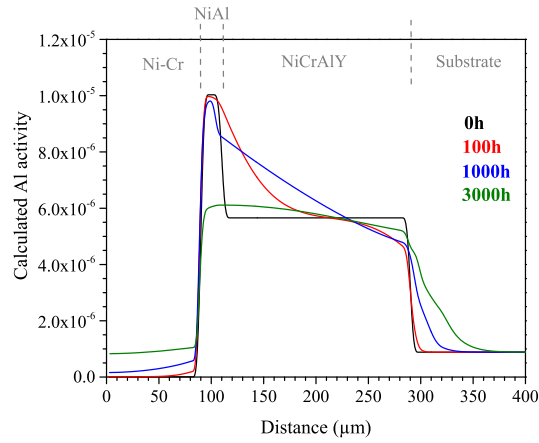


Figure 8: Calculated phase distribution in the material of the as-received coating on CMSX-4 based on the nominal compositions of each of the coating layers and the substrate CMSX-4. The dotted lines show the position of the interfaces between the layers at  $t=0$ .

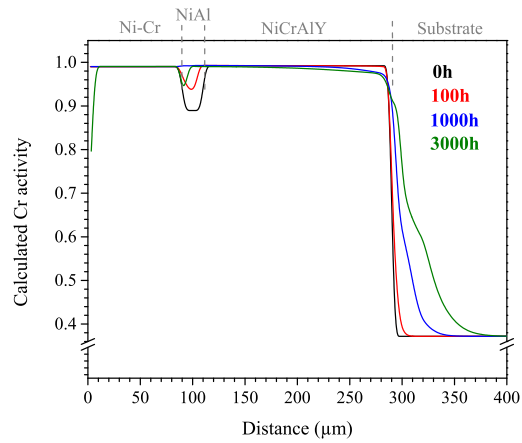




(a)



(b)



(c)

Figure 9: Activity profiles of (a) Ni, (b) Al and (c) Cr calculated with ThermoCalc (TCNI5) in the as-received state ( $t=0$ ) and after 100 h, 1000 h and 3000 h of discontinuous exposure at 800 °C.

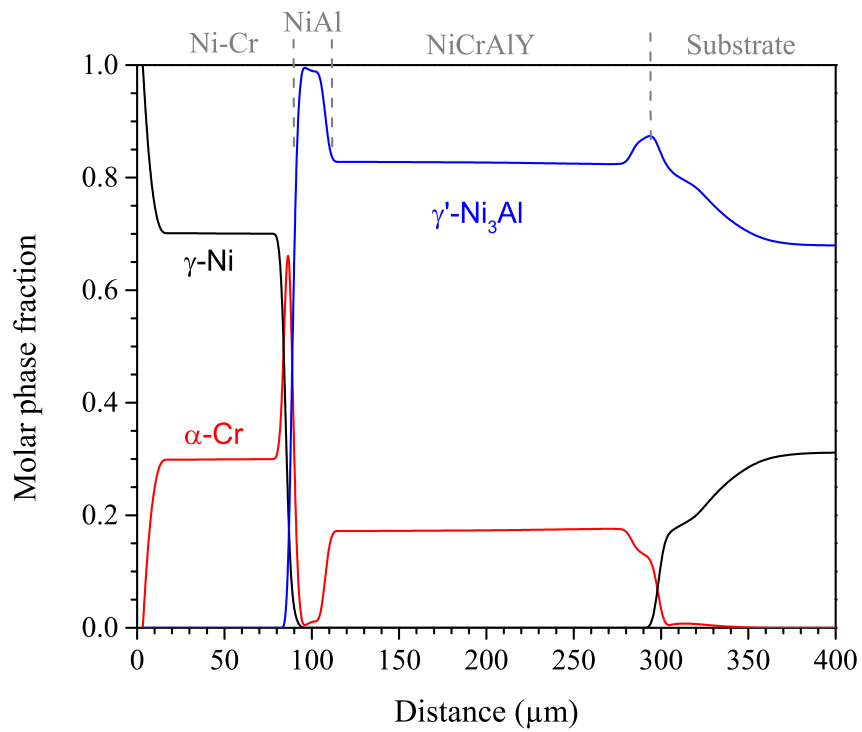


Figure 10: Calculated phase distribution in the multilayered coating on CMSX-4 after discontinuous exposure at 800 °C for 3000 h in laboratory air. The dotted lines show the position of the interfaces between the layers at  $t=0$ .

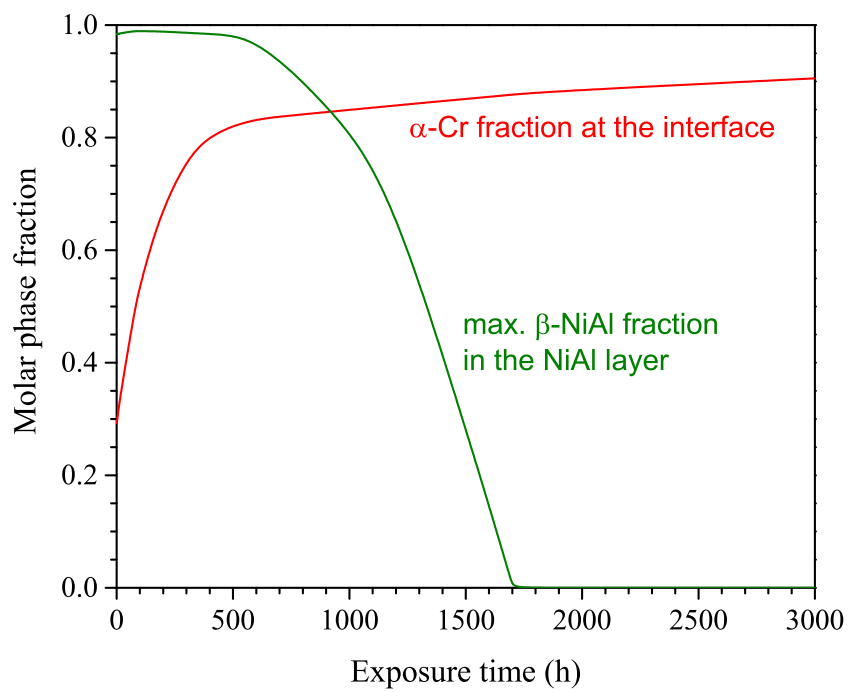


Figure 11: Temporal evolution of the calculated maximum  $\beta$ -NiAl molar phase fraction in the aluminide layer and the  $\alpha$ -Cr molar phase fraction at the interface between the Ni-Cr and aluminide layers during discontinuous exposure at 800 °C in laboratory air.

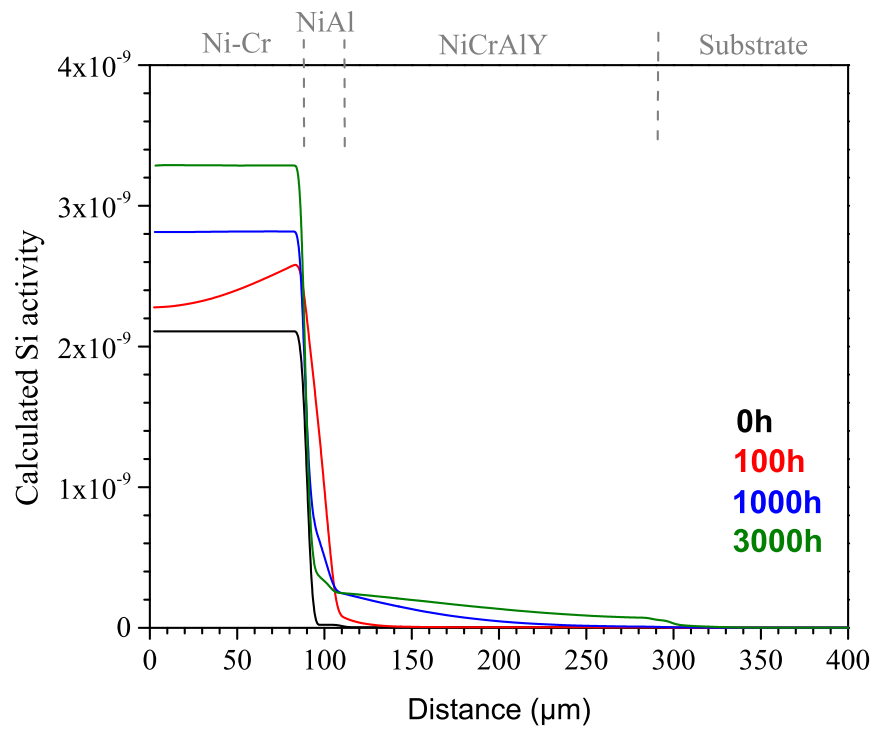
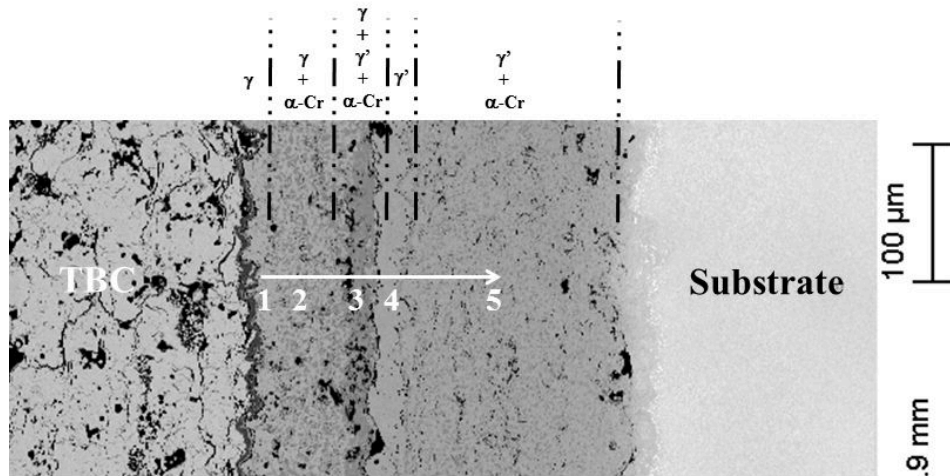
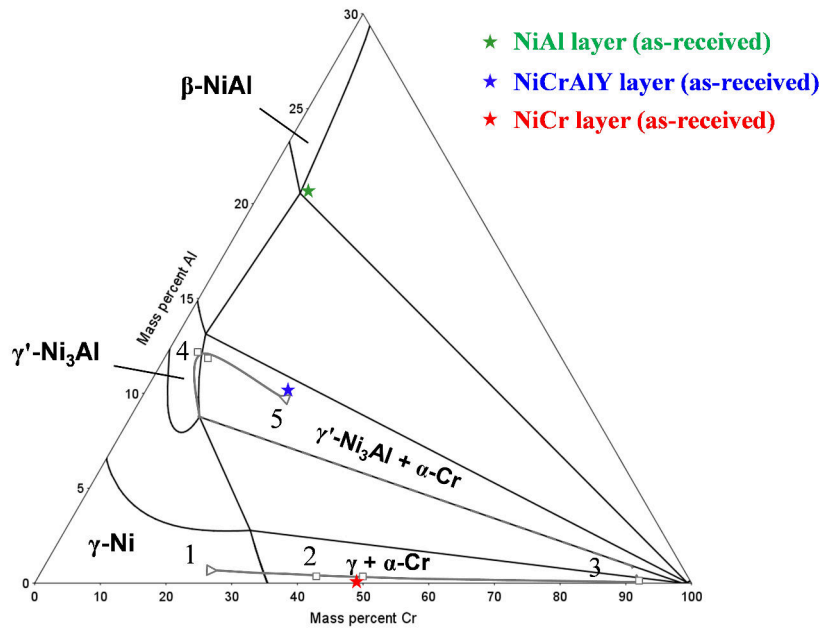


Figure 12: Activity profiles of Si calculated with ThermoCalc (TCNI5) in the as-received state ( $t=0$ ) and after 100 h, 1000 h and 3000 h of discontinuous exposure at 800 °C.



(a)



(b)

Figure 13: (a) BSE-image showing the positions of the compositions in the individual layers after discontinuous exposure in air for 3000 h at 800 °C in the material multilayered coating on CMSX-4. (b) Diffusion paths moving from the sub-surface region (Position 1) to the NiCrAlY layer (Position 5) on the calculated ternary Ni-Cr-Al isothermal section.